

RSC Advances



This is an *Accepted Manuscript*, which has been through the Royal Society of Chemistry peer review process and has been accepted for publication.

Accepted Manuscripts are published online shortly after acceptance, before technical editing, formatting and proof reading. Using this free service, authors can make their results available to the community, in citable form, before we publish the edited article. This *Accepted Manuscript* will be replaced by the edited, formatted and paginated article as soon as this is available.

You can find more information about *Accepted Manuscripts* in the [Information for Authors](#).

Please note that technical editing may introduce minor changes to the text and/or graphics, which may alter content. The journal's standard [Terms & Conditions](#) and the [Ethical guidelines](#) still apply. In no event shall the Royal Society of Chemistry be held responsible for any errors or omissions in this *Accepted Manuscript* or any consequences arising from the use of any information it contains.



Journal Name

ARTICLE

Electrochemical Sensing of Hydrazine using Multilayer Graphene Nanobelts

Received 00th January 20xx,
Accepted 00th January 20xx

Padmanathan Karthick Kannan^a, Stainslav A. Moshkalev^b and Chandra Sekhar Rout^{a,*}

DOI: 10.1039/x0xx00000x

www.rsc.org/

Abstract. The electrochemical sensing property of multi-layer graphene nanobelts (GNB) towards hydrazine is studied. The developed hydrazine sensor showed the sensitivity value of $0.08 \mu\text{A } \mu\text{M}^{-1} \text{cm}^2$ with a linear range of $10 \mu\text{M}$ to 1.36 mM . The interference data also exhibited high selectivity to hydrazine even in the presence of common interfering species like ascorbic acid, uric acid, glucose and lactic acid.

1. Introduction

Hydrazine is a highly toxic and carcinogenic chemical which has been widely used in many industrial and pharmaceutical applications including rocket propellant, explosives, herbicides, corrosion inhibitor and oxygen scavenger¹. Although, hydrazine has lots of potential applications, its long-term exposure to human beings can cause severe serious health problems. Exposure towards high concentrations of hydrazine leads to different health problems including brain and DNA damage, deterioration of central nervous system while low concentration creates dizziness, irritation of eyes, nose and throat². World Health Organization (W.H.O) has classified hydrazine as group B2 human carcinogens³. Therefore, it is very much important to develop sensor for the sensitive detection of low and high concentrations of hydrazine in both environmental and industrial sectors. A plethora of methods including conductometry⁴, electrochemical⁵, colorimetry⁶ and fluorescent⁷ have been extensively employed for the detection of hydrazine. Among these methods, electrochemical based sensors find potential attention widely attracted because of their high selectivity, sensitivity, low detection limit, wide linear range, stability, reproducibility, simplicity and low cost⁸.

A variety of nanomaterials including nanostructured metals and

metal nanoparticles^{9–12} nano-conducting polymers^{13,14} have been widely explored in electrochemical sensor application during the past few decades. In addition to the aforementioned materials, carbon nanomaterials such as carbon nanofiber, carbon nanotube (CNT), carbon nano horn and graphene have also been used in electrochemical sensors due to their high-quality crystal lattices, high carrier mobility and low noise^{15–17}. Among these, graphene has attracted huge attention among researchers since 2004 because of its unusual structural characteristics, electronic flexibility and attractive physical and chemical properties^{18,19}.

Moreover, graphene based nanomaterials are believed to provide a new path for the development of high performance electrochemical sensors due to their enhanced electrochemical active surface area and good electron transport property²⁰. Very recently, there has been an immense interest on the use of novel graphene nanostructures like ultra-thin graphene nanoflakes, graphene nanoribbons as an electrode material because of its high specific surface area compared to single exfoliated graphene sheet and carbon nanotube^{21–24}. Furthermore, these nanostructures have edge defects and can be expected to show more reactivity towards chemical species compared to pristine graphene. However, these novel graphene nanostructures have been scantily explored on the development of electrochemical sensors. Yuan *et al.* investigated the electrochemical properties of graphene samples with both basal and edge plane defects and found that edge plane samples show high electron transfer rate and strong electrocatalytic activity compared to the basal one²⁵. With this objective, the present study aimed to develop an electrochemical sensor for the detection of hydrazine using multilayer graphene nanobelts (GNB). The schematic of GNB based electrochemical hydrazine sensor used in the present study and its sensing mechanism is shown in Fig. 1. To the best of our knowledge, there has been no report on the use of GNB in electrochemical hydrazine sensors. For the first time, the as-synthesized GNB is used as an active material for the electrochemical detection of hydrazine.

^a School of Basic Sciences, Indian Institute of Technology Bhubaneswar, Bhubaneswar, Odisha – 751013. E-mail: csrout@iitbbs.ac.in, pkk.matsci@gmail.com

^b Center for Semiconductor Components, State University of Campinas, Campinas, Sao Paulo, 13083-870, Brazil

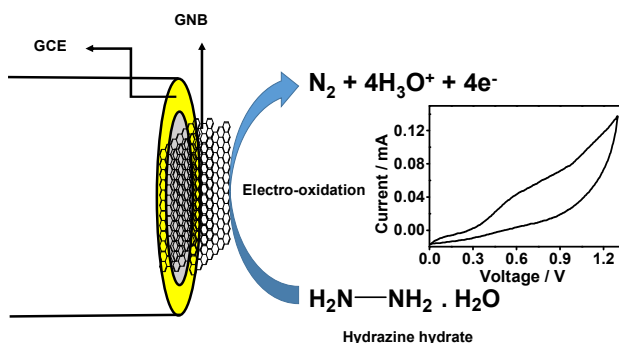


Fig. 1 Schematic representation of hydrazine sensing mechanism at GNB/GCE

2. Experimental methods.

2.1 Synthesis of Graphene Nanobelts (GNB):

Natural graphite was obtained from Nacional de Grafite, Brazil and used as received. GNB was prepared by adopting the method already reported in the literature²⁶. Briefly, a required amount of graphite was dispersed in 100 ml of isopropanol (volume: 1 mg/mL) for 2 hrs using an ultrasonic bath and subsequently dried in an incubator for further use. Details of the synthesis process can be found elsewhere²⁷.

2.2 Characterization Techniques and Electrochemical Measurements :

The surface morphology of the GNB samples were analysed by Field-Emission Scanning Electron Microscopy (FESEM) MERLIN Compact with GEMINI I electron column, Zeiss Pvt. Ltd., Germany). Raman spectra were obtained by using Micro-Raman spectroscopy in confocal configuration (NT-MDT NTEGRA Spectra, with 473 nm laser source). All the electrochemical measurements were performed using PG262A potentiostat/galvanostat (Technosience Ltd., Bangalore, India). A conventional three-electrode cell consisting of a glassy carbon electrode (GCE) (CHI104, CH Instruments Inc, USA) as the working electrode. A saturated Ag/AgCl and a Pt wire were used as the reference and counter electrode respectively. All the experiments were performed at room temperature ($25 \pm 1^\circ \text{C}$). 0.1 M phosphate buffer solution (PBS) with the pH value of 7 was used as the supporting electrolyte. Amperometric experiments were carried out under continuous stirred condition by applying a potential of 0.5 V vs Ag/AgCl.

2.3 Preparation of GNB modified GCE (GNB/GCE):

Prior to modification, glassy carbon electrode (GCE) was first cleaned by using $1\ \mu\text{m}$ and $0.05\ \mu\text{m}$ alumina powders. Generally, alumina powder with the particle size of $0.05\ \mu\text{m}$ is used to remove the scratches on the electrode surface. However, in order to make the electrode surface very uniform without any scratches and also to get rid of surface impurities, alumina powder with a particle size of $1\ \mu\text{m}$ is also used in the present study. After polishing, the electrode is cleaned by sonication in water and ethanol for 5 min

respectively. As-prepared GNB was dispersed by sonication in ethanol (1 mg/ mL) for 30 min to form a homogenous dispersion. Then, $5\ \mu\text{L}$ of the GNB dispersion was drop cast onto the GCE surface and dried at room temperature for 10 min to obtain GNB/GCE.

3. Results and Discussion

3.1. Microscopic and spectroscopic characterization of GNB:

Fig. 2A, B show the FESEM images of as-prepared GNB. The images show very thin flakes of GNB in different dimensions with large amount of active edges. The presence of active edges on the GNB surface is expected to play an important role for the electron transfer processes during the electrochemical detection of the analytes²⁸. FESEM image also shows a number of wrinkles on GNB surface which actually help to facilitate the electron transfer processes²⁹. Fig. 2C shows the Raman spectral data of GNB. The spectrum shows a peak at $1357\ \text{cm}^{-1}$ corresponding to D band which indicates that the as-synthesized GNB has very low defect density³⁰. Another two peaks at $1581\ \text{cm}^{-1}$ and $2720\ \text{cm}^{-1}$ corresponding to the presence of characteristic G and 2D bands of graphene respectively. The total number of layers present on the graphene surface can be easily determined from the relative intensity ratio between G and 2D band i.e. $I_G/I_{2D} < 1$ for single layer graphene and $I_G/I_{2D} > 1$ for few-layer graphene and this value normally increases with increasing number of layers. In the present study, the value of I_G/I_{2D} is estimated to be 2.2. This observation inferred that the as-prepared GNB consists of multilayers of graphene^{31,32}.

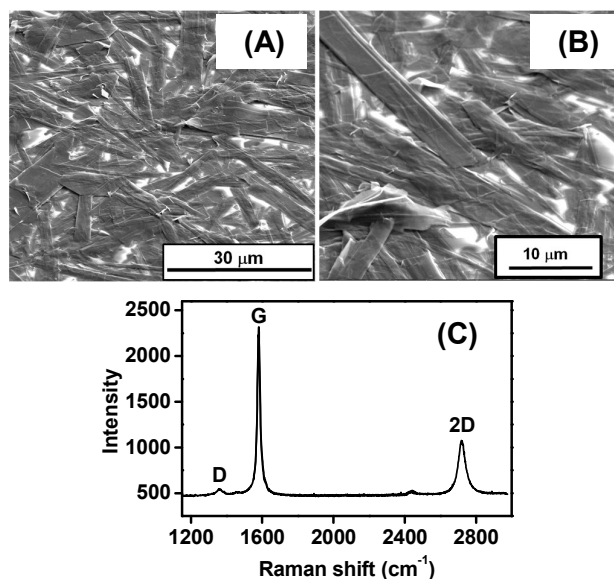


Fig. 2 Two SEM images taken with different magnification, showing randomly oriented nanobelts. Scale bar: (A) $30\ \mu\text{m}$ and (B) $10\ \mu\text{m}$. (C) RAMAN spectrum of as-prepared GNB measured by using 473

nm laser showing three peaks; D band – 1357 cm^{-1} ; G band – 1581 cm^{-1} ; 2D band – 2720 cm^{-1} .

3.2. Electrochemical behaviour of GNB/GCE:

The electrochemical properties of GNB/GCE were investigated by performing cyclic voltammetry (CV) measurements in a solution containing 5 mM potassium ferrocyanide and 0.1 M KCl at a scan rate of 40 mV s^{-1} (Fig. 3A). It can be observed from the data that bare GCE shows a couple of redox peaks with the peak to peak potential difference value (ΔE_p) of 112 mV. On the other hand, GNB/GCE shows enhanced redox peak currents with ΔE_p value of 67 mV. The large difference in the ΔE_p value has been attributed to the large surface to volume ratio and high electrical conductivity of the GNB. The interfacial properties of GNB/GCE were further characterized by performing electrochemical impedance spectroscopy measurements. Fig. 3B shows the Nyquist plots of bare and GNB modified GCE measured in 5mM potassium ferricyanide solution containing 0.1 M KCl. It can be seen that a small semicircle with a straight line is observed for bare GCE in high and low-frequency regions respectively. While GNB/GCE shows a straight line in the low-frequency region with a depressed semicircle in the high-frequency region (top inset of Fig. 3B).

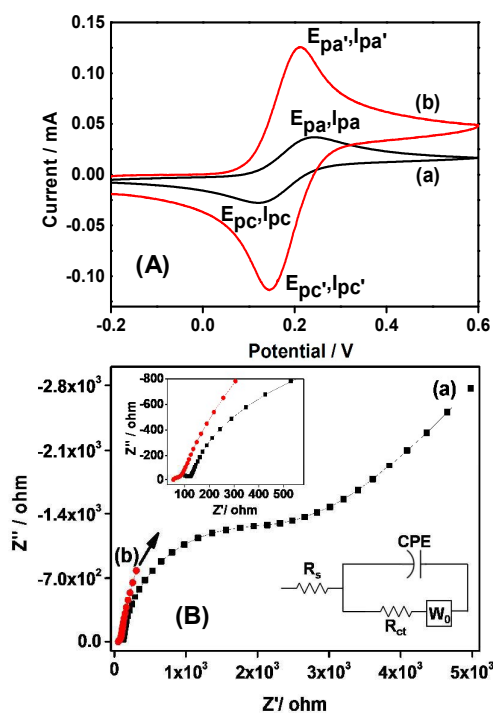


Fig. 3 (A) CV data of (a) bare GCE ($E_{pa} = 242$ mV; $E_{pc} = 120$ mV; $i_{pa} = 36.8$ μA ; $i_{pc} = 27.8$ μA) and (b) GNB/GCE ($E_{pa}' = 213$ mV; $E_{pc}' = 146$ mV; $i_{pa}' = 125.4$ μA ; $i_{pc}' = 113.4$ μA) measured in 0.1 M KCl solution containing 5 mM potassium ferrocyanide, scan rate - 40 mV s^{-1} . (B) Nyquist plots of bare GCE and GNB/GCE measured in 0.1 M KCl solution containing 5 mM potassium ferrocyanide. Top inset is the

expanded view of Nyquist plot obtained for GNB/GCE and bottom inset is the fitted equivalent circuit

Further, the impedance data were analyzed by fitting it with standard equivalent circuit models in order to extract the electrical parameters. The most satisfactory circuit model for the measured impedance data is shown as bottom inset of Fig. 3B consisting of solution resistance (R_s) connected in series to the parallel combination of the constant phase element (CPE) and charge transfer resistance (R_{ct}) in series with the Warburg impedance (W_0). The extracted values of R_{ct} correspond to bare and GNB/GCE are 2.4 k Ω and 40 Ω respectively. These values imply that unmodified GCE shows large interfacial impedance value and when it is modified with GNB, the R_{ct} value tremendously decreased, indicating that GNB possesses high electrical conductivity which could accelerate the electron transfer reaction between the electrode and electrolyte interface. Thus, the as-prepared GNB is expected to act as a suitable material for the sensitive determination of hydrazine.

3.3 Electrochemical sensing property of GNB/GCE towards hydrazine:

In order to ascertain the sensing property of GNB/GCE towards hydrazine, CV measurements were performed. Fig. 4 shows the CVs of bare GCE and GNB/GCE in the absence and presence of 1mM hydrazine in 0.1 M PBS at a scan rate of 40 mV s^{-1} . In blank phosphate buffer solution (PBS), bare GCE and GNB/GCE does not show any characteristic peak in the measured voltage range. Meanwhile addition of hydrazine generated a negligible amount of oxidation current in bare GCE without any characteristic peaks indicating the poor electrocatalytic ability towards hydrazine oxidation. When 1mM hydrazine was added, GNB/GCE exhibited a large oxidation peak at 0.6 V in the potential range between 0.4 and 0.8 V. The existence of peak with large oxidation current in the presence of hydrazine clearly suggests that the GNB/GCE showed good electrocatalytic property towards hydrazine.

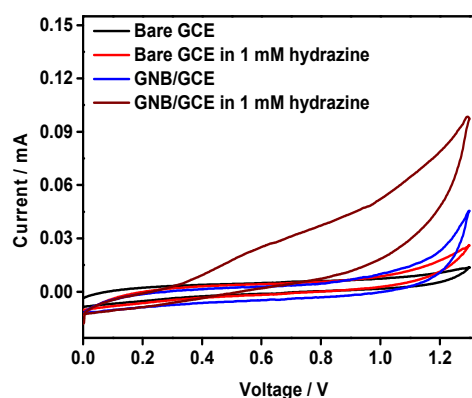


Fig. 4 Comparative CV data of GCE and GNB/GCE in the presence and absence of 1 mM hydrazine in 0.1M PBS (pH 7). Scan rate: 40 mV s^{-1} .

The scan rate dependence on the electrochemical response of GNB/GCE towards hydrazine oxidation has been investigated and

the results are shown in Fig. 5A. The scan rate dependence experiments were performed in 0.1M PBS containing 1mM hydrazine at various scan rates using CV technique. The observed CVs at different scan rates indicate that by increasing the scan rate, the oxidation peak current (I_p) increases correspondingly suggesting that the oxidation process occurring at the surface of GNB electrode is a diffusion controlled one. Fig. 5B shows a plot of oxidation peak current (I_p) against the square root of the scan rate which exhibits a linear relationship between the two parameters that again confirms the occurrence of diffusion controlled electron transfer process³³ on the GNB/GCE surface. The corresponding linear equation can be represented by Eq. 1

$$I_p(\text{mA}) = 0.0034 \left(v^{1/2} \right) (\text{mV}^{1/2} \text{s}^{-1}) + 0.0036 \quad (1)$$

For a completely irreversible diffusion controlled processes, the relation between the oxidation peak current (I_p) and the square root of the scan rate ($v^{1/2}$) can be expressed as Eq. 2³³

$$I_p = (2.99 \times 10^5) n [(1 - \alpha)n_a]^{1/2} A C_0 D_0^{1/2} v^{1/2} \quad (2)$$

where n is the number of electrons involved in the overall hydrazine oxidation process, α is the electron transfer coefficient, n_a is the number of electrons transferred in the rate determining step, A is the electrode area (0.07 cm^2), C_0 is the bulk concentration of hydrazine ($0.1 \times 10^{-3} \text{ mol m}^{-3}$).

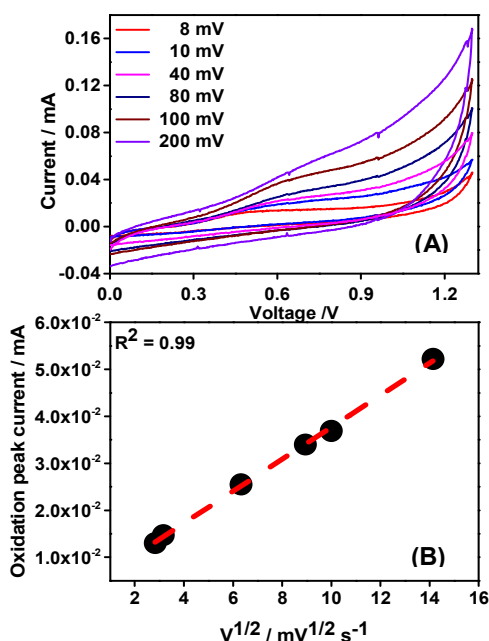
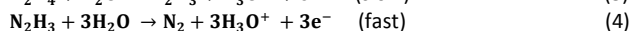
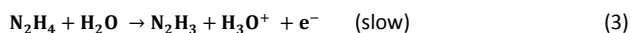


Fig. 5 CV data of GNB/GCE measured in 0.1 M PBS (pH 7) containing 1 mM hydrazine at different scan rates. (d) Linear plot of oxidation peak current against the square root of scan rate

By considering the reported value of D_0 and $(1-\alpha)n_a$ for graphene as $2.2 \times 10^{-5} \text{ cm}^2 \text{ s}^{-1}$ and 0.48^{22,28}, the number of electrons transferred in the hydrazine oxidation processes (n) can be calculated using Eq. (2) and it is found to be 4. From the above observation, it is inferred that the overall hydrazine oxidation involves four- electrons transfer which is consistent with the

literature reports³⁴ and the reaction mechanism can be represented by Eqs. 3 and 4.



Here, the first equation is the rate determining slow step in which one electron transfer is involved followed by a fast second step involving three electron transfer processes. Thus, the overall hydrazine oxidation reaction can be expressed by Eq. 5.

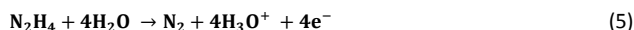


Fig. 6 shows the chrono-amperometric response of GNB/GCE on successive addition of different concentrations of hydrazine in 0.1M PBS solution at a constant potential of 0.5 V. Upon each addition of hydrazine, the developed sensor exhibited quick and sensitive response. The response of the sensor achieved a steady state within 10 s (ESI Fig. S1) indicating the fast electrocatalytic behaviour of GNB. From the amperometric response data, a calibration plot was constructed by plotting concentration of hydrazine against oxidation current. From the data (Fig. 6B), it has been observed that the oxidation peak current (I_p) increases linearly with increase in hydrazine concentration.

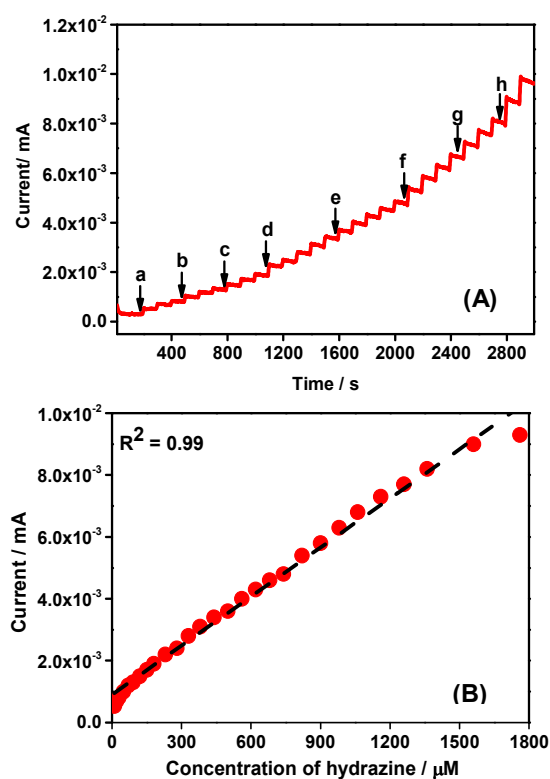


Fig. 6 (A) Chrono-amperometric response of GNB/GCE upon successive addition of different concentrations of hydrazine (in μM) (a) 10 (b) 20 (c) 30 (d) 50 (e) 60 (f) 80 (g) 100 (h) 200 into 0.1 M PBS (pH 7) at 0.5 V. (B) Calibration plot of the hydrazine sensor with the fitted linear equation $I_p(\text{mA}) = 5.3 \times 10^{-6} [\text{hydrazine}](\mu\text{M}) + 9.1 \times 10^{-4}$

The limit of detection (LOD) and limit of quantification (LOQ) of the amperometric hydrazine sensor were calculated as described in³⁵ which are found to be to be 1.13 μM and 3.76 μM respectively and the sensitivity value is estimated to be 0.075 $\mu\text{A } \mu\text{M}^{-1} \text{cm}^{-2}$. The stability of GNB/GCE towards hydrazine electrochemical oxidation was ascertained by recording 100 consecutive cyclic voltammograms in 0.1M PBS containing 2mM hydrazine at a scan rate of 40 mV s^{-1} . It was estimated that about 85% of the oxidation current was retained in the 100th cycle indicating that the developed GNB based hydrazine sensor showed superior stability during the entire process. Two types of structural defects are believed to be present in graphene sheets viz. basal and edge which are reported to exhibit two different electrochemical properties. Graphene sheets with edge plane are found to exhibit superior electrochemical performances compared to the basal plane²⁵. In order to compare the performance of GNB in the present study with the reported sensors based on other nanomaterials and graphene modified electrodes, a table has been compiled which is shown in ESI (Table 1). From the table, it is evident that the developed GNB sensor shows good performance in terms of high sensitivity and good linear range^{22,29,36-40}. It is also worth mentioning that the developed sensor shows long range linearity in the concentration range between 10 μM and 1.3 mM. Thus, the detection of hydrazine at low and high domain can be easily achieved by employing GNB which will be very helpful to develop sensors in both public and industrial sectors. These observations clearly revealed the role of edge defects on enhancing the electrochemical performance of graphene-based sensors.

The influence of some electroactive species on the sensing property of GNB/GCE towards hydrazine was investigated by performing amperometry measurements. Fig. 7 shows the amperometric responses of GNB/GCE for the successive addition of different concentrations of hydrazine and 50 μM uric acid, dopamine, ascorbic acid, glucose and lactic acid at a regular interval of 100 s in 0.1 M PBS at an applied potential value of 0.5 V.

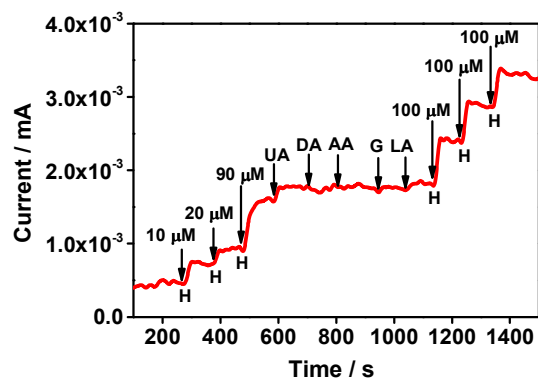


Fig. 7 Interference study of GNB/GCE in 0.1 M PBS with different concentrations of hydrazine: a1 – 10 μM , a2 – 20 μM , a3 – 90 μM , a4 – 100 μM in the presence of 50 μM (b) uric acid, (c) dopamine (d) ascorbic acid (e) glucose and (f) lactic acid. Applied potential - 0.5 V.

It can be observed from the plot that upon the addition of hydrazine, the increase in current value was observed which is further increases with increase in hydrazine concentration. In a similar way, the addition of glucose and uric acid also increase the current response to a negligible extent (< 5 %). However, no significant change in the current value was observed during the addition of 50 μM of other interfering species. Hence, GNB/GCE shows sensitive and selective response towards hydrazine even in the presence of various co-existing interfering species thus exhibiting its good selectivity.

Conclusions

The electrochemical sensing properties of GNB towards hydrazine were investigated. Larger surface area and enhanced electrochemical properties due to large number of active edges played important role for the detection of low concentration of hydrazine. The developed GNB based hydrazine sensor showed high sensitivity value of 0.080 $\mu\text{A } \mu\text{M}^{-1} \text{cm}^{-2}$ with a LOD value of 1.1 μM . Thus, GNB emerge as an active material for the electrochemical sensing of hydrazine and this work opens a way to develop practical hydrazine sensors for various environmental and industrial applications.

PKK and CSR gratefully acknowledge the support of the University Grant commission, India-UK-India Education and Research Initiative (UGC-UKIERI, Grant No. UGC-2013-14/005). SAM acknowledges the support by CNPq (Brazil).

References

- 1 J. E. Troyan, *Ind. Eng. Chem.*, 1953, **45**, 2608–2612.
- 2 G. Choudhary and H. Hansen, *Chemosphere*, 1998, **37**, 801–843.
- 3 N. Rastakhiz, A. Kariminik, V. Soltani-Nejad and S. Roodsaz, *Int. J. Electrochem. Sci.*, 2010, **5**, 1203–1212.
- 4 S. Kumar, G. Bhanjana, N. Dilbaghi and A. Umar, *Ceram. Int.*, 2015, **41**, 3101–3108.
- 5 P. V Dudin, P. R. Unwin and J. V Macpherson, *Phys. Chem. Chem. Phys.*, 2011, **13**, 17146–17152.
- 6 M. Sun, J. Guo, Q. Yang, N. Xiao and Y. Li, *J. Mater. Chem. B*, 2014, **2**, 1846–1851.
- 7 Y. Sun, D. Zhao, S. Fan and L. Duan, *Sensors Actuators B Chem.*, 2015, **208**, 512–517.
- 8 F. Faridbod, V. K. Gupta and H. A. Zamani, *Int. J. Electrochem.*, 2012, **2011**.
- 9 J. Zhang and C. M. Li, *Chem. Soc. Rev.*, 2012, **41**, 7016–7031.
- 10 S. Guo and E. Wang, *Nano Today*, 2011, **6**, 240–264.
- 11 A. Umar, M. M. Rahman, S. H. Kim and Y.-B. Hahn, *Chem. Commun.*, 2008, 166–168.

COMMUNICATION

Journal Name

- 12 S. Reddy, B. E. K. Swamy and H. Jayadevappa, *Electrochim. Acta*, 2012, **61**, 78–86.
- 13 S. Virji, R. B. Kaner and B. H. Weiller, *Chem. Mater.*, 2005, **17**, 1256–1260.
- 14 B. Fabre and L. Taillebois, *Chem. Commun.*, 2003, 2982–2983.
- 15 X. Mao, G. C. Rutledge and T. A. Hatton, *Nano Today*, 2014, **9**, 405–432.
- 16 H. Dai, L. Gong, G. Xu, S. Zhang, S. Lu, Y. Jiang, Y. Lin, L. Guo and G. Chen, *Electrochim. Acta*, 2013, **111**, 57–63.
- 17 G. Xu, L. Gong, H. Dai, X. Li, S. Zhang, S. Lu, Y. Lin, J. Chen, Y. Tong and G. Chen, *Anal. Methods*, 2013, **5**, 3328–3333.
- 18 P. Avouris and C. Dimitrakopoulos, *Mater. today*, 2012, **15**, 86–97.
- 19 W. Choi, I. Lahiri, R. Seelaboyina and Y. S. Kang, *Crit. Rev. Solid State Mater. Sci.*, 2010, **35**, 52–71.
- 20 S. Wu, Q. He, C. Tan, Y. Wang and H. Zhang, *Small*, 2013, **9**, 1160–1172.
- 21 O. J. Yoon, C. H. Kim, I.-Y. Sohn and N.-E. Lee, *Sensors Actuators B Chem.*, 2013, **188**, 454–461.
- 22 S. Mutyala and J. Mathiyarasu, *Sensors Actuators B Chem.*, 2015, **210**, 692–699.
- 23 N. S. Ismail, Q. H. Le, H. Yoshikawa, M. Saito and E. Tamiya, *Electrochim. Acta*, 2014, **146**, 98–105.
- 24 A. Martín, J. Hernández-Ferrer, M. T. Martínez and A. Escarpa, *Electrochim. Acta*, 2015, **172**, 2–6.
- 25 W. Yuan, Y. Zhou, Y. Li, C. Li, H. Peng, J. Zhang, Z. Liu, L. Dai and G. Shi, *Sci. Rep.*, 2013, **3**.
- 26 F. P. Rouxinol, R. V. Gelamo, R. G. Amici, A. R. Vaz and S. A. Moshkalev, *Appl. Phys. Lett.*, 2010, **97**, 253104.
- 27 Nacional de Grafite Ltda, Itapecerica, MG, Brazil (http://grafite.com/inicio_en.asp#)
- 28 Y. Wang, Y. Wan and D. Zhang, *Electrochem. commun.*, 2010, **12**, 187–190.
- 29 C. Wang, L. Zhang, Z. Guo, J. Xu, H. Wang, K. Zhai and X. Zhuo, *Microchim. Acta*, 2010, **169**, 1–6.
- 30 S. C. Bodepudi, A. P. Singh and S. Pramanik, *Electronics*, 2013, **2**, 315–331.
- 31 X. Dong, Y. Ma, G. Zhu, Y. Huang, J. Wang, M. B. Chan-Park, L. Wang, W. Huang and P. Chen, *J. Mater. Chem.*, 2012, **22**, 17044–17048.
- 32 A. Reina, X. Jia, J. Ho, D. Nezhich, H. Son, V. Bulovic, M. S. Dresselhaus and J. Kong, *Nano Lett.*, 2009, **9**, 30–35.
- 33 A. J. Bard and L. R. Faulkner, *Electrochem. Methods*, 2nd ed.; Wiley New York, 2001.
- 34 J. Li, H. Xie and L. Chen, *Sensors Actuators B Chem.*, 2011, **153**, 239–245.
- 35 P. K. Kannan and C. S. Rout, *Chem. – A Eur. J.*, 2015, **21**, 9355–9359.
- 36 H. R. Zare and N. Nasirizadeh, *Electrochim. Acta*, 2007, **52**, 4153–4160.
- 37 L. Zheng and J. Song, *Sensors Actuators B Chem.*, 2009, **135**, 650–655.
- 38 M. A. Kamyabi, O. Narimani and H. H. Monfared, *J. Electroanal. Chem.*, 2010, **644**, 67–73.
- 39 S. Shukla, S. Chaudhary, A. Umar, G. R. Chaudhary and S. K. Mehta, *Sensors Actuators B Chem.*, 2014, **196**, 231–237.
- 40 S. P. Kim and H. C. Choi, *Sensors Actuators B Chem.*, 2015, **207**, 424–429.